Cerebral Cortex, December 2016;26: 4497–4512

doi: 10.1093/cercor/bhw327
Advance Access Publication Date: 25 October 2016
Original Article

ORIGINAL ARTICLE

The Organization of Mouse and Human Cortico-Hippocampal Networks Estimated by Intrinsic Functional Connectivity

Eyal Bergmann, Gil Zur, Guy Bershadsky, and Itamar Kahn

Department of Neuroscience, Rappaport Faculty of Medicine, Technion – Israel Institute of Technology, Haifa 31096, Israel

Address correspondence to Itamar Kahn, Department of Neuroscience, Rappaport Faculty of Medicine, Technion – Israel Institute of Technology, 1 Efron St., POB 9649 Bat Galim, Haifa 31096, Israel. Email: kahn@technion.ac.il

Abstract

While the hippocampal memory system has been relatively conserved across mammals, the cerebral cortex has undergone massive expansion. A central question in brain evolution is how cortical development affected the nature of cortical inputs to the hippocampus. To address this question, we compared cortico-hippocampal connectivity using intrinsic functional connectivity MRI (fcMRI) in awake mice and humans. We found that fcMRI recapitulates anatomical connectivity, demonstrating sensory mapping within the mouse parahippocampal region. Moreover, we identified a similar topographical modality-specific organization along the longitudinal axis of the mouse hippocampus, indicating that sensory information arriving at the hippocampus is only partly integrated. Finally, comparing cortico-hippocampal connectivity across species, we discovered preferential hippocampal connectivity of sensory cortical networks in mice compared with preferential connectivity of association cortical networks in humans. Supporting this observation in humans but not in mice, sensory and association cortical networks are connected to spatially distinct subregions within the parahippocampal region. Collectively, these findings indicate that sensory cortical networks are coupled to the mouse but not the human hippocampal memory system, suggesting that the emergence of expanded and new association areas in humans resulted in the rerouting of cortical information flow and dissociation of primary sensory cortices from the hippocampus.

Key words: hippocampus, mammalian brain evolution, mouse connectivity atlas, mouse fMRI, resting state

Introduction

The hippocampal memory system has been suggested to be well conserved during evolution, demonstrating both structural and functional similarities across species, particularly in mammals (Manns and Eichenbaum 2006; Allen and Fortin 2013). However, other neural structures have undergone significant changes during evolution and are remarkably different in primates. The most radical changes occurred in the cerebral cortex, demonstrating numerous structural, molecular and genetic evolutionary differences in development and organization (Rakic 2009; Geschwind and Rakic 2013). These differences underlie the massive elaboration of the cortex in primates, and the incorporation of expanded and new high-order perceptual and association areas (Buckner and Krienen 2013). Since the hippocampus receives inputs from all parts of the cerebral cortex via structures within the parahippocampal region (Eichenbaum 2000; Ranganath and Ritchey 2012), it is possible that information processing in the evolved cortex has changed the nature of cortical inputs to the

hippocampus, and as a result, the nature of its function to support qualitatively different memory-guided computations.

Previous studies described a conserved organization of the hippocampal memory system, demonstrating 2 parallel streams of cortical inputs in both rodents and primates (Ranganath and Ritchey 2012; Ho and Burwell 2014). These pathways are anatomically (Suzuki 2009; van Strien et al. 2009) and functionally (Norman and Eacott 2005; Kahn et al. 2008; Neunuebel et al. 2013; Navarro Schröder et al. 2015) distinct as object-related information flows to the perirhinal (PRC) and lateral entorhinal (LEC) cortices, while context-related information flows to the posthrinal/parahippocmpal (POR/PHC) and medial entorhinal (MEC) cortices. These 2 streams are combined in the hippocampus (Kerr et al. 2007), but interconnections also exist in the parahippocampal region (Burwell and Amaral 1998a). Therefore, the anatomy of the cortico-hippocampal system is best described as including both parallel and hierarchical components, positioning it well to integrate diverse informational sources important to episodic memory.

Despite the radical evolutionary changes in the cerebral cortex, anatomical tracing studies in rats and monkeys described a homologous cortical information flow to the hippocampus (Burwell and Agster 2008; Suzuki 2009). In both species, most inputs arrive at the parahippocampal region from high-order sensory and polymodal association cortices, although direct projections from primary sensory areas were reported in rodents (Burwell and Amaral 1998b; Burwell 2000; Aronoff et al. 2010; Wang et al. 2012). Neuroimaging studies in humans described functional connectivity between the hippocampal memory system and the anterior temporal and posterior medial association networks (Kahn et al. 2008; Libby et al. 2012; Ranganath and Ritchey 2012). Previous characterization of cortico-hippocampal functional connectivity in rodents focused on association cortical systems demonstrating putative homology to humans (Lu et al. 2012; Schwarz et al. 2013; Gass et al. 2014; Mechling et al. 2014; Liska et al. 2015). However, functional connectivity between sensory cortical systems and the hippocampus has not been characterized. Taking into account that cortical elaboration in primates, specifically humans, changed the balance between sensory and association cortices (Buckner and Krienen 2013), it is possible that despite the similar anatomical connectivity of sensory cortices to the hippocampus, functional connectivity differs across species, supporting qualitatively different sensory inputs to the hippocampus.

In this study, we sought to compare cortico-hippocampal connectivity in awake mouse and human brains using intrinsic functional connectivity MRI (fcMRI). This method estimates functional connectivity by measuring correlations of slow spontaneous fluctuations in the blood oxygenation level-dependent (BOLD) fMRI signal across brain regions (Buckner et al. 2013; Power et al. 2014b). In mice, we identified spatially localized organization of different sensory modalities in the parahippocampal region that extends to the hippocampus. In addition, we discovered preferential connectivity of primary and high-order sensory cortices over cortical association areas in the hippocampal memory system. In contrast, in the human hippocampal memory system, we found preferential connectivity of association rather than sensory cortical networks, as well as spatial divergence of these networks in the parahippocampal region. These results indicate divergent functional organization of the cortico-hippocampal circuit in mice and humans, suggesting that sensory information in humans is rerouted via expanded and new association cortices before arriving at the hippocampus.

Materials and Methods

Ethics

All animal procedures were conducted in accordance with the ethical guidelines of the National Institutes of Health, and were approved by the Institutional Animal Care and Use Committee (IACUC) at the Technion. Human participants provided written-informed consent in accordance with guidelines set forth by the Institutional Review Board of the Massachusetts General Hospital.

Animals

Twelve male C57BL/6 mice (8–12 weeks old) were implanted with MRI-compatible head-posts and housed in reversed 12 h light/dark cycle in groups of 2 or 3 animals per cage. After 3 d of recovery, a 7–10 d training period was started to acclimatize the animals to the head fixation. The mice then underwent multiple 45-min-long awake head-fixed fcMRI sessions (Supplementary Table 1).

Head-Post Surgery

For the head fixation, a custom-made MRI-compatible head-post was implanted over the skull. Mice were anesthetized with isoflurane (1.5–2.5%), mounted on a surgical frame and kept on a thermal blanket (FHC) to maintain body temperature. Analgesia was administrated locally (Bupivacaine) and systematically (Buprenorphine), and eye ointment (Duratears, Alcon-Couvreur) was applied to prevent dryness. The scalp and periosteum over the entire surface of the skull were removed in order to improve adhesion and prevent susceptibility artifacts. After chemical etching, the head-post was attached to the skull using dental cement (C&B Metabond, Parkell). In some cases, another layer of dental cement (Paladur, Heraeus Kulzer) was applied to create a homogenous surface and reduce the effect of susceptibility artifacts. An intramuscular injection of broad-spectrum antibiotics (Penicillin-Streptomycin) was given to prevent postoperative infections. Mice were given at least 3 d to recover and received edible Buprenorphine gel daily before behavioral acclimatization commenced.

Acclimatization to Awake Head-Fixed Imaging

To achieve extended stable recording in the mice during passive wakefulness, we designed an MRI-compatible cradle (Fig. 1A) and acclimatized the animals to the head fixation before the experiment started to reduce stress and head motion (Desai et al. 2011; Guo et al. 2014). The procedure started with 5 handling sessions performed over 3–5 d in which the mice became familiar with the experimenter. Then, the mice were head-fixed for gradually longer periods (2, 5, 10 and 25 min) over 4 d. Each session was performed at approximately the same time of day (late afternoon), and included brief anesthesia with isoflurane (5%), attachment to the cradle under a low concentration of isoflurane (0.5–1%) and an acclimatization period inside the MRI scanner. The fMRI protocol was used to acclimatize the mice to the scanner noise and possible effects of the gradients; no noticeable startled or freezing responses nor changes in breathing patterns were observed, suggesting that the mice were oblivious to the imaging procedure. At the end of each session, the mice received food reward.

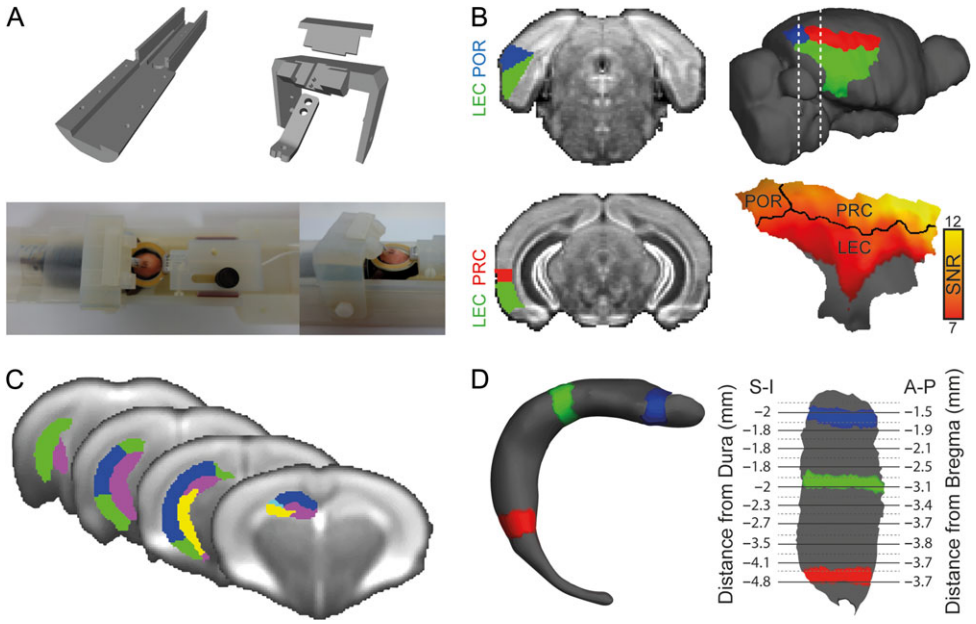

Figure 1. Visualization of fMRI results in mice. (*A*) Experimental setup for awake mouse fMRI: custom-made 3D-printed cradle for fMRI in awake head-fixed mice (top); a head-fixed mouse is shown in the cradle with a 20 mm receive-only loop-coil located above the head (bottom). (*B*) Segmentation of the mouse parahippocampal region in the AMBC Atlas (left) and on a surface reconstruction of the mouse cortex (right). SNR map of the parahippocampal region is presented on the surface reconstruction showing high SNR in the PRC and POR, and attenuated SNR in the LEC due to susceptibility artifacts originating from the air–tissue interface near the ear canals. (*C*) AMBC Atlas derived segmentation of the hippocampus into subfields overlaid on the group average BOLD SE-EPI upsampled to 100 µm isotropic resolution. (*D*) Three-dimensional surface reconstruction of the right dentate gyrus (left) and flattened surface representation of the right dentate gyrus (right); colored segments show the relationships between the surfaces. Coordinates in the Atlas space are provided for the flattened representation, superior–inferior (S-I) relative to the dura and anterior–posterior (A-P) relative to bregma.

Mouse Image Acquisition

MRI scans were performed at 9.4 T MRI (Bruker BioSpin GmbH) using a quadrature 86 mm transmit-only coil and a 20 mm loop receive-only coil (Bruker). After brief anesthesia (5% isoflurane), the mice were mounted on the cradle. A low concentration of isoflurane (0.5–1%) was used to maintain anesthesia until placement in the scanner. Total exposure to isoflurane lasted up to 5 min and the animals had at least 15 min to recover during scanner calibrations. Each session included acquisition of one low-resolution rapid acquisition process with a relaxation enhancement (RARE) T1-weighted structural volume (time repetition [TR] = 1500 ms, time echo [TE] = 8.5 ms, RARE-factor = 4, flip angle [FA] = 180°, 30 coronal slices, 150 × 150 × 450 µm^3 voxels, no interslice gap, FOV 19.2 × 19.2 mm^2, matrix size of 128 × 128) and 4 spin echo EPI (SE-EPI) runs with 200 time points measuring BOLD fluctuations (TR = 2500 ms, TE = 18.398 ms, FA = 90°, 30 coronal slices, 150 × 150 × 450 µm^3 voxels, no interslice gap, FOV 14.4 × 9.6 mm^2, matrix size of 128 × 128). In addition, one high-resolution Turbo-RARE T2-weighted volume was acquired for each mouse during the last acclimatization session (TR = 6000 ms, TE = 12 ms, RARE-factor = 8, FA = 180°, 50 coronal slices; 100 × 100 × 300 µm^3 voxels, no interslice gap, FOV 38.4 × 38.4 mm^2, matrix size of 384 × 384). After excluding 32 sessions with image distortions or substantial movement (less than 7 min of data available after motion scrubbing), a total of 100 sessions were included in the analysis.

Mouse Anatomical Data

The Allen Mouse Brain Connectivity (AMBC) Atlas (Lein et al. 2007; Oh et al. 2014), including atlas labels and anatomical tracing results, was downloaded from the Allen Brain Institute website at 100 µm^3 resolution and converted to NIFTI format. The Allen Histology Atlas was then manually downsampled to the functional data resolution (150 × 150 × 450 µm^3) and a conversion matrix between the original and the downsampled versions was created. To register functional data to the atlas, 3 high-resolution anatomical scans were aligned manually to the downsampled atlas, averaged and then used as a target for registration of the functional data. Subsequently, the inverse conversion matrix was used for registration of functional data to the original atlas and anatomical connectivity database.

Mouse Data Preprocessing Procedure

Standard mouse fMRI preprocessing was based on the work of Kahn et al. (2011), and included removal of the first 2 volumes for T1-equilibration effects, compensation of slice-dependent time shifts, rigid body correction for head motion, linear transformation for registration to the AMBC Atlas (Supplementary Fig. 1) and intensity normalization. Preprocessing of fcMRI data was performed based on a standard human protocol (Power et al. 2014a) with the exception of whole-brain signal regression, which was found to dramatically reduce correlations without any increase in specificity (Supplementary Fig. 2). This preprocessing procedure yielded excellent homotopic connectivity, which is the hallmark of fcMRI in rodents (Gozzi and Schwarz 2016).

First, a data-scrubbing procedure was conducted to eliminate motion artifacts (Power et al. 2014a). Exclusion criteria included frame displacement of 50 µm, temporal derivative root mean square variance over voxels (DVARS) of 0.5% and exclusion of 2 frames before and one after the detected movement. Examination of motion patterns (Supplementary Fig. 3) indicated that animal movement occurred over sequential frames, and

excluded frames were distributed across animals. Comparison between scrubbed and unscrubbed data reveals that motion scrubbing significantly reduces variability between sessions with high and low motion. In addition, we found that as opposed to humans (Power et al. 2014a), motion in mice decreases signal similarity between white matter and other brain compartments. Further analysis revealed that motion is correlated positively with the white matter signal and negatively with the ventricles and whole-brain signals. Finally, motion scrubbing specifically increased the similarity between white matter and other brain compartments. Taking into account the location of the corpus callosum between cortical and subcortical structures and its relatively small volume, this result suggests that regression of the white matter signal reduces the negative effects of motion artifacts in the mouse.

After motion scrubbing, data underwent demeaning and detrending, as well as regression of motion parameters and average time courses in the ventricles and white matter (from the included frames only) to eliminate motion-related and physiological noise. Finally, a temporal filter was used to isolate the low frequency spectrum ($0.009 < f < 0.08$ Hz), and spatial smoothing with a Gaussian kernel with FWHM of 450 μm was applied to improve the temporal signal-to-noise ratio (SNR), which was estimated for each BOLD run by dividing the mean value of each voxel by its standard deviation.

Mouse fcMRI Analysis

To estimate functional connectivity, 450 μm-diameter spheres (5 voxels) were defined as seed regions and placed in sensory ($n = 24$) and association ($n = 13$) cortices throughout the mouse cortex (Supplementary Table 2). For large regions, several seeds were placed within the area and data were averaged across seeds, resulting in a total of 9 sensory and 7 association regions. Seed locations were determined based on the AMBC Atlas according to injection sites estimated by downsampling the anatomical optical density maps to the space of the functional data. In order to prevent partial volume effects of signals from noncortical structures or from outside the brain, the seeds were placed in the middle of the cortical ribbon. The time course of each seed was extracted and used to calculate seed-based Fisher's Z transformed r values (Zar 1996). For the group analysis, the correlation maps of each animal were averaged, resulting in 12 average maps that were submitted to a one-way t-test (SPM, Wellcome Department of Cognitive Neurology, London, UK). The statistical threshold was determined using family-wise error rate correction for multiple comparisons in the whole brain (excluding olfactory bulb, brainstem, and cerebellum), or in the hippocampal memory system, bilaterally including the hippocampus and parahippocampal region. For seed-to-seed analyses, the average Fisher's Z transformed r values were calculated in the specific region of interest to compare the region's connectivity to other brain areas.

Characterization of Structure–Function Relations in the Mouse Brain

To estimate the voxel-wise overlap between functional and anatomical connectivity, we compared optical density maps that approximate anatomical connectivity to functional connectivity maps generated from the seed region located at the center of the injection site. To eliminate the confounding effects of colocalization of the injection site and seed region, a 2 mm-diameter sphere around the seed center was excluded from the analysis. We then binarized both maps based on the statistical threshold for the functional map ($P < 0.05$, corrected for multiple comparisons for the whole brain) and the optical density threshold for the anatomical map. The optical density threshold of 0.1 was chosen since it was shown that a false-positive rate reaches a plateau and stabilizes at around zero for this value (Oh et al. 2014). It is important to note that anatomical connectivity as expressed by optical density maps does not discriminate between fibers of passage and terminal zones, creating an overestimation of anatomical connectivity and limiting the precise estimation of structure–function relations. After generating these binary maps, we estimated the overlap between them using the Sørensen–Dice index ($D = 2 \times (A \cap B) / (|A| + |B|)$). To allow for a meaningful interpretation of this estimate, we compared it to the expected index calculated based on the expected overlap of the 2 maps. Finally, to examine the consistency of structure–function relations across the group, we replicated the functional analyses at a single animal level using a $Z(r)$ correlation threshold of 0.04.

To compare anatomical and functional connectivity at a regional level, normalized projection volumes were taken from the supplementary materials published by Oh et al. (2014). Statistically reliable functional volumes were calculated for each brain region using the AMBC Atlas labels. Due to limitations of functional resolution, small areas (<0.05 mm^3, ~5 voxels at functional resolution) and areas with poor SNR (<7, before smoothing) were excluded from this analysis. The resulting anatomical and functional connectivity matrices were used for characterization of structure–function relations. First, we sorted the functional connectivity volume distribution in a descending order and examined the coverage of the 20 strongest anatomical connections in the rank-ordered functional connections. Then, to test structure–function relations in many cortical areas and across multiple statistical thresholds, we used the anatomical data as a baseline and generated a series of receiver operating characteristic (ROC) curves. We used a volume threshold of 0.05 mm^3 to define binary anatomical connections, and then calculated the functional volume distribution over 82 statistical thresholds to examine the sensitivity and specificity of the prediction of functional connections based on anatomical connections. To estimate the accuracy of the prediction, we calculated the area under each ROC curve, which estimates the relationship between true-positive and false-positive predictions at different thresholds, indicating how well anatomical connectivity discriminates between functionally connected and unconnected regions.

Mouse Surface Reconstruction

Surface reconstructions were created using FreeSurfer software (Dale et al. 1999). The AMBC Atlas at 100 μm^3 was used to construct superficial (pial) and deep (white) surfaces based on masks of the whole brain including or excluding the cerebral cortex, respectively. Each vertex (the equivalent of a voxel in surface space) in the deep surface was matched to the closest vertex in the superficial surface to coalign the surfaces. The alignment product was defined as the deep layer (white) of the superficial surface allowing the definition of the cortical ribbon. Anatomical labels and optical density at isotropic 100 μm^3 resolution, and correlation and statistical maps at $150 \times 150 \times 450$ μm^3 were registered to the surface. Validating the registration process, we found that by setting the projection fraction to 1, the surface represented layer 5, which is a good estimate of the functional data in which there is no layer-specificity. In addition, functional data were smoothed in the surface space

using a Gaussian kernel with FWHM of 100 μm. For the anatomical data, each volume was registered with projection distances of 300 and 700 μm to represent both superficial and deep layers, respectively, and the 2 registered files were averaged.

Segmentation of the mouse parahippocampal region was based on the AMBC Atlas (Fig. 1*B*). However, this atlas lacks a specific definition of the postrhinal cortex and instead defines the ectorhinal (area 36) and perhinal (area 35) cortices. Therefore, we used a previous anatomical work on mice (Beaudin et al. 2013) and defined the POR as the part of the ectorhinal label that is caudal to the perirhinal label, and the PRC as the perirhinal label and part of the ectorhinal label that is not included in the postrhinal cortex definition. Examination of the SNR in the parahippocampal region revealed attenuation of signal in LEC (Fig. 1*B*). The compromised SNR is due to susceptibility artifacts originating from the air–tissue interface near the ear canal, limiting the interpretation of results in the LEC, but allowing examination of functional connectivity along most of the rostro-caudal axis of the PRC and POR. By projecting the fcMRI statistical maps and anatomical optical density maps of different sensory cortices on the surface reconstruction, we were able to visualize the precise topographical organization of sensory modalities within the parahippocampal region.

For visualization of the mouse hippocampus, we used specific labels from the AMBC Atlas (Fig. 1*C*) to create 3D surfaces of the different hippocampal subfields (for illustration, the dentate gyrus is shown in Fig. 1*D*). Here, the superficial and deep surfaces were defined based on masks of the whole subfield and its deeper layer only, and functional data were smoothed in the surface space using a Gaussian kernel with FWHM of 100 μm and registered with a projection fraction of zero since the data are visible on both aspects of the surface. To create a flat representation (Fischl et al. 1999), a longitudinal cut was made in the medial aspect of each subfield and saved as a patch. This patch was then flattened to create a 2D representation (Fig. 1*D*), which reliably represents the original volume-based statistical maps (Supplementary Fig. 4).

To enable transformations of the functional maps into a coordinate space that can be used in future imaging and electrophysiological studies targeting specific sites identified here, we report the data in the Paxinos and Franklin (2001) and AMBC Atlas coordinate systems. To estimate stereotactic coordinates in the flattened hippocampal surfaces, we loaded the surface coordinates to Matlab (The Mathworks), and divided them into 25 segments along a perpendicular line (Supplementary Fig. 5). We then found the vertices that are most proximal to the center of gravity of each segment and extracted their volume-based coordinates in the original AMBC Atlas using the volume/surface visualizer (TkMedit). In the AMBC Atlas, we estimated the distance of each center of gravity from the dura and bregma. Since the AMBC Atlas does not contain a stereotactic coordinate system, dura location was defined based on the highest point in the cortex and bregma was anatomically identified based on Paxinos and Franklin (2001). Since the hippocampal surfaces were cut in the medial aspect before flattening, the center of gravity represents the most superficial layers: the superior and lateral aspects of the dorsal and ventral areas, respectively. Therefore, another few hundred microns are needed to locate the center of each subfield, for example, for electrophysiological measurements.

Human fcMRI

Human data were taken from Dataset 2 of Kahn et al. (2008) and comprised 44 participants (age 22.22 ± 2.82, 19–32 [mean ± SD, range] years old; 27 females). Participants were scanned using a 3 T (TimTrio Siemens) with a 12-channel phased-array head coil. For each participant, 2 runs of 76 time points were acquired (GE-EPI, TR = 5000 ms, TE = 30 ms, FA = 90°, 55 axial slices, $2 \times 2 \times 2\,mm^3$ voxels, no interslice gap, FOV $256 \times 256\,mm^2$, matrix size of 128×128). Data preprocessing steps included removal of the first 4 volumes, compensation of slice-dependent time shifts and rigid body correction for head motion. Functional images were then transformed linearly to a downsampled version of the Montreal Neurological Institute (MNI) template at $2 \times 2 \times 2\,mm^3$. fcMRI preprocessing was identical to the procedure in mice except for the additional step of whole-brain signal regression, as well as adjustments of motion scrubbing threshold for displacement to 0.5 mm and a Gaussian kernel for smoothing to 4 mm. Note that unlike the original publication (Kahn et al. 2008), here a more conservative treatment of motion was carried out (Power et al. 2014a).

To calculate the hippocampal and parahippocampal coverage of different cortical systems, time courses were extracted from functional seeds (spheres; 3 mm radius; 7 voxels × $2\,mm^3$ = 56 mm^3 volume) taken from the meta-analysis of Power et al. (2011), which was used for grouping of seeds to cortical systems. Out of the 264 seeds, 106 were chosen by restricting the analysis to the left hemisphere and excluding noncortical seeds (Supplementary Table 3). In addition, seeds within the parahippocampal region were also excluded from the analysis. For each seed, volume-based correlation maps were submitted to a one-way *t*-test. A lenient threshold was set to prevent false-negative correlations of sensory regions ($P < 0.001$, uncorrected for multiple comparisons). For surface representation, the final statistical maps were registered to the "fsaverage" cortical surface template (Fischl et al. 1999). Visualization of the parahippocampal region was based on surface reconstruction of the medial temporal lobe as described in Kahn et al. (2008).

Estimation of Hippocampal and Parahippocampal Coverage Across Species

To compare cortical functional connectivity to the hippocampal memory system across species, we segmented the hippocampus and parahippocampal region and calculated the fraction of significant voxels in each structure for different seeds. In the mouse, we used our PRC and POR labels to segment the parahippocampal region, but excluded the entorhinal cortex and the superficial parts of the PRC and POR labels due to poor SNR (<7). The mouse hippocampus was defined based on the AMBC Atlas and included the dentate gyrus, CA3, CA2, CA1 and subiculum; voxels with SNR lower than 7 were excluded. In humans, we registered the FreeSurfer segmentation of the hippocampus, parahippocampal cortex and perirhinal/entorhinal cortex to a downsampled MNI space at $2 \times 2 \times 2\,mm^3$.

Results

Anatomical Connections Predict Functional Connectivity in Awake Mice

Cortical networks diverge in how much they conform to a pure hierarchical organization (e.g., sensory vs. association). Since fcMRI measures both monosynaptic and polysynaptic connections, we sought to establish that it could be used to characterize the cortical organization of networks that are not predominantly hierarchical. We compared a functional connectivity map (Fig. 2*A*) generated by a seed region in the barrel-related

primary somatosensory cortex (SSp-bfd) to efferent anatomical projections of this region (Fig. 2B) and found that 38.61% of the significant functional connectivity voxels and 7.67% of the voxels above the optical density threshold overlap (Fig. 2C), yielding a Sørensen–Dice index of 0.128. Based on the brain coverage of functional (4.13%) and anatomical (20.8%) maps, we found that the expected Sørensen–Dice index is 0.069, resulting in an observed-to-expected ratio of 1.858 and suggesting preferential functional connectivity in voxels that are strongly connected anatomically. To formally test this result and examine individual variability in structure–function relations, we calculated the average correlation map for each animal and used a binary correlation threshold of 0.04 to examine reproducibility (Fig. 2D). We then calculated the observed-to-expected ratios of the Sørensen–Dice indices across the group and found that they are significantly greater than 1 (1.15 ± 0.1, mean ± SD; unpaired 2-tailed t-test: $t_{(11)} = 5.14$, $P < 0.001$), formally indicating that voxels that are strongly connected anatomically are more likely to be connected functionally. Next, we sought to test whether functional connectivity is more reproducible in voxels having strong anatomical connections. Therefore, we examined the individual coverage of group-level significant functional connectivity voxels compared between voxels above (79.47% ± 12.22%, mean ± SD) and below (71.74% ± 14.14%, mean ± SD) the optical density threshold (Fig. 2E), and found significantly higher coverage in voxels above the threshold (paired 2-tailed t-test: $t_{(11)} = 8.3$, $P < 0.001$), indicating higher reproducibility.

To examine structure–function relations at the regional level, we compared brain-wide volume distributions of functional and anatomical connections. We sorted brain-wide SSp-bfd functional connections to create a rank-ordered array of connections and counted the number of ranks needed to cover the 20 strongest anatomical connections (Fig. 2F, Supplementary Table 4). We found that 10 and 19 out of the 20 strongest anatomical connections were covered within 13 and 60 strongest functional connections, respectively. Since larger regions are generally characterized by higher connection volumes, we sought to estimate the contribution of region size to the results. Therefore, we calculated the coverage of the anatomical connections in a rank-ordered array of region sizes and found that it covers only 6 and 17 anatomical connections within the 13 and 60 largest regions, respectively, underperforming functional connectivity measures. To formally test these results, we shuffled the anatomical data 10 000 times and randomly chose 20 connections each time (controlling for the mean regional size of the connections to be higher than the mean of the veridical 20 anatomical connections). We then replicated this analysis with random anatomical connections (Fig. 2G) and found that the coverage is lower than the original analysis ($P < 0.001$), indicating that anatomically connected regions are more likely to be functionally connected.

Next, we sought to characterize structure–function relations in all cortical systems by evaluating the extent to which anatomical connections predict functional connectivity over multiple statistical thresholds. We computed ROC curves for 37 cortical seeds, grouping for 13 association areas (Fig. 2H) and 24 primary and secondary sensory areas (Fig. 2I). We found that the area under the curve for each ROC (auROC), which measures the ability of anatomical connectivity to classify regions as functionally connected or unconnected, was greater than chance (0.5) in all cases. Comparing auROC values between association and sensory cortices (Fig. 2J), we found that they are reliably higher in sensory relative to association regions (unpaired 2-tailed t-test, $t_{(35)} = 3.31$, $P = 0.002$), indicating that structure–function relations are distinguished between these networks.

Our findings are in close agreement with a recent study reporting that anatomical connectivity predicts fcMRI results in anesthetized mice based on whole-brain connectivity matrices (Stafford et al. 2014). Here, we were able to replicate this finding in awake mice and extend the analysis by comparing structure–function relations between different cortical systems. Next, we sought to evaluate this result in detail, focusing on cortico-hippocampal connectivity.

Sensory Mapping in the Mouse Parahippocampal Region

Previous anatomical tracing studies in rats described topographic organization of primary and secondary sensory areas of different modalities within the parahippocampal region (Burwell and Amaral 1998b; Furtak et al. 2007). Therefore, utilizing fcMRI and the AMBC Atlas, we sought to examine whether such mapping exists in the mouse parahippocampal region, whether functional connectivity recapitulates anatomical connectivity patterns and how it relates to connectivity of association cortices.

Examination of the fcMRI results revealed sensory mapping within the parahippocampal region (Fig. 3A), with the primary visual cortex (VISp) connected mainly to the POR, the primary auditory cortex (AUDp) connected to all PRC, especially to the intermediate part, and the SSp-bfd connected mainly to the rostral but also the caudal PRC. Comparing the fcMRI results to anatomical connections (Fig. 3B), we found close agreement in spatial specificity between the 2 imaging modalities, as both demonstrated distinct topographical organization. Volume-based quantification along the longitudinal axis (Fig. 3C) validates the surface-based representation of the functional and anatomical data. To formally test for topographical organization, we grouped the correlation values along the longitudinal axis to 4 sections and submitted the results to a repeated-measures ANOVA (corrected with the Huynh-Feldt method) with Seed Region as a within animal factor and correlation values of the 4 Longitudinal Sections as repeated measures. This analysis revealed significant interaction between Seed Region and Longitudinal Sections ($F_{(6,\ 22)} = 15.15$, $P < 0.001$, $\varepsilon_{H\text{-}F} = 1$). Post-hoc tests revealed that this interaction applies to all pairs of cortical seeds (visual-auditory: $F_{(3,11)} = 20.75$, $P < 0.001$, $\varepsilon_{H\text{-}F} = 0.963$; visual-somatosensory: $F_{(3,\ 11)} = 5.47$, $P = 0.014$, $\varepsilon_{H\text{-}F} = 1$; auditory-somatosensory: $F_{(3,11)} = 15.94$, $P < 0.001$, $\varepsilon_{H\text{-}F} = 0.855$), indicating sensory mapping.

Replicating the analysis for seeds in association cortices, we observed weaker functional connectivity and anatomical connections (examples of retrosplenial and anterior cingulate cortices are shown in Fig. 3D, E). To examine the spatial characteristics of sensory and association seeds, we grouped the 37 seeds to regions (9 sensory, 7 association), averaged the statistical maps in each region, and calculated the statistically significant fraction of sensory and association regions for each parahippocampal vertex. We found exclusive representation of primary sensory cortices in most parts of the PRC, with no evidence of spatial divergence between sensory and association cortices (Fig. 3F). Characterization of the anatomical connectivity for these regions supports this finding (Fig. 3G). Taken together, our results show dominancy of sensory over association networks within the mouse parahippocampal region. Moreover, they indicate that while different sensory modalities

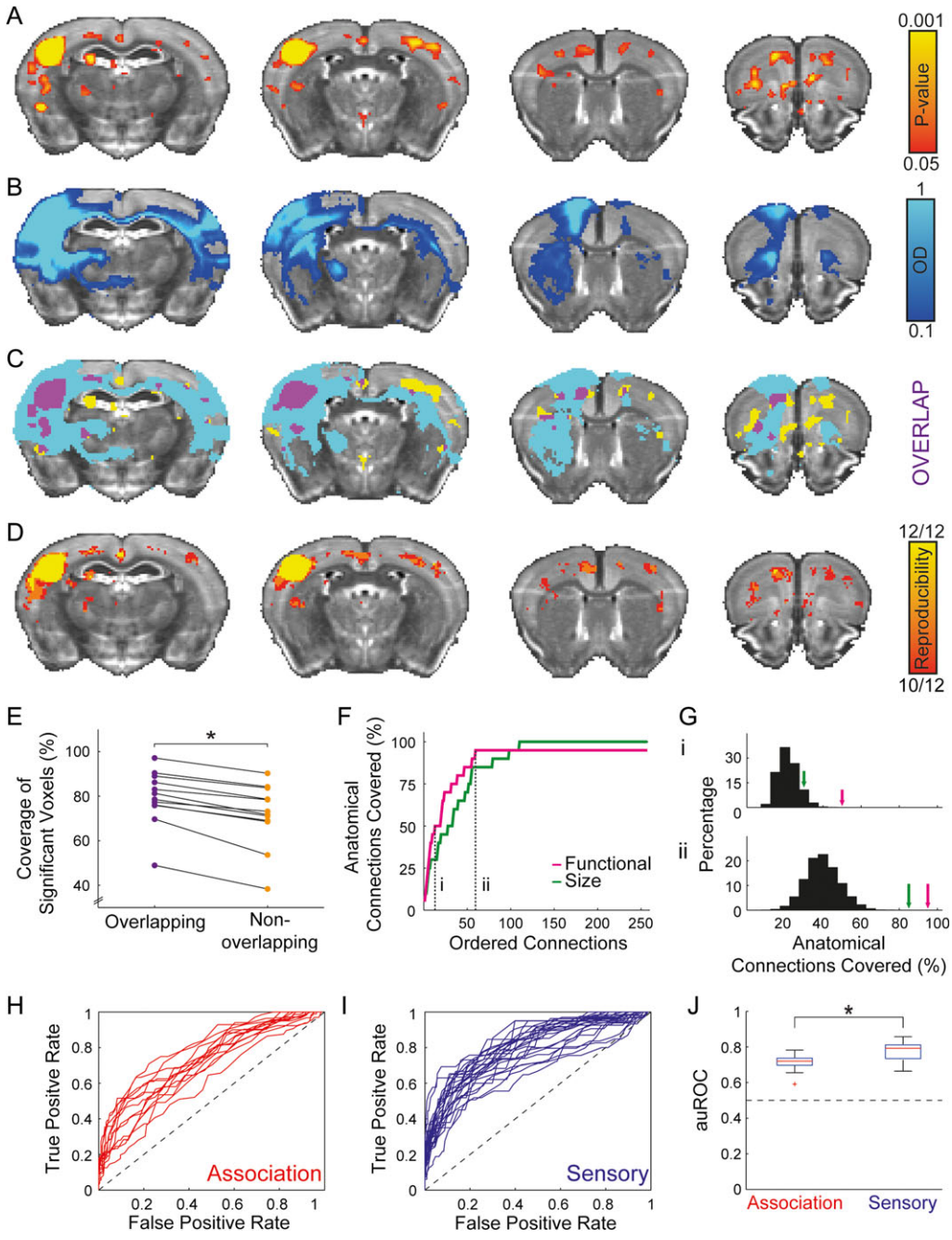

Figure 2. Structure–function relations in the mouse cortical somatosensory network. (*A*) A statistical parametric map (in red-yellow) of positive correlations of barrel-related primary somatosensory cortex (SSp-bfd) upsampled to AMBC Atlas at 100 μm^3 resolution; $P < 0.05$, corrected for multiple comparisons using family-wise error rate correction for the whole mouse brain. (*B*) Anatomical connections (optical density, [OD] in blue-light blue) of SSp-bfd taken from the AMBC Atlas experiment #112951804, normalized OD > 0.1. (*C*) Overlap of functional and anatomical connectivity (purple) demonstrates a close agreement across the 2 modalities. (*D*) Estimation of reproducibility of functional connectivity demonstrates strong structure–function relations across animals. Average correlation maps were calculated for each animal; a binary threshold of 0.04 was used to estimate the overlap between animals. (*E*) Examination of the coverage of group-level statistically significant functional connectivity in individual animals as a function of the overlap with anatomical connectivity demonstrates higher reproducibility in overlapping voxels. (*F*) Within the somatosensory network, we quantified the coverage of the top 20 anatomical connections of SSp-bfd as a function of the rank-ordered SSp-bfd seed region's functional connections (purple) and region sizes (green). The graph indicates 19 out of 20 anatomical connections recapitulated by the functional connections (full results are detailed in Supplementary Table 4). AMBC Atlas labels with poor SNR (<7) or volume below the functional resolution acquisition (<0.05 mm^3) were excluded from this analysis. (*G*) Distributions of the number of shuffled anatomical connections covered in rank-ordered functional array for the 13th (i) and 60th (ii) ranks compared to the number of veridical anatomical connections covered in functional and region-size arrays. (*H*, *I*) ROC curves demonstrate that functional connectivity is predicted by anatomical connectivity for both association (*H*) and sensory (*I*) cortices. (*J*) auROC curve is plotted for the 2 classes of cortical regions, revealing weaker structure–function relations in association relative to sensory cortices (central mark is the median, the edges of the box are the 25th and 75th percentiles, the whiskers extend to the most extreme data points not considered outliers, and outliers are plotted individually).

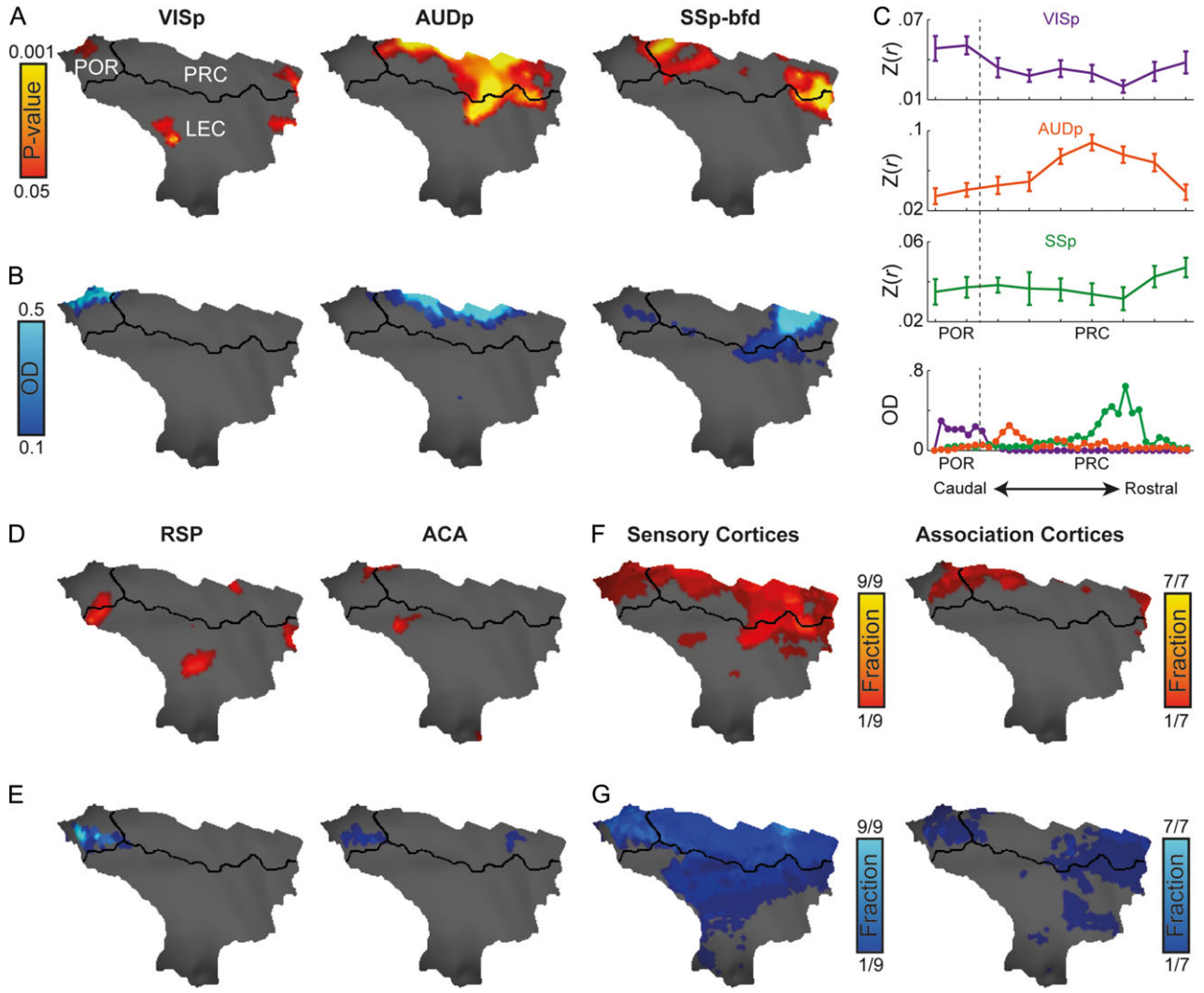

Figure 3. Convergence of sensory and association networks as opposed to spatially localized sensory mapping in the mouse parahippocampal region. (*A*) Functional connectivity of primary visual (VISp, left), auditory (AUDp, center) and barrel-related somatosensory (SSp-bfd, right) cortices and parahippocampal region, $P < 0.05$ corrected for multiple comparisons using family-wise error rate correction for the hippocampal memory system. (*B*) Anatomical connections between primary visual, auditory, and somatosensory cortices and the parahippocampal region. (*C*) Volume-based quantification of the average correlations (top) and normalized optical density (bottom) of different sensory modalities along the longitudinal axis of the parahippocampal region. Error bars indicate standard error of the mean. Functional (*D*) and anatomical connectivity (*E*) of the retorsplenial (RSP, left) and anterior cingulate (ACA, right) cortices in the parahippocampal region (similar to *C*, *D*). Functional (*F*) and anatomical (*G*) fractions of sensory (left) and association (right) regions cover the mouse parahippocampal region. In regions that contain several seeds, the functional and anatomical maps were averaged; same thresholds from (*A*, *D*) and (*B*, *E*) were used as binary thresholds for the functional and anatomical data, respectively.

are organized topographically along the rostro-caudal axis, association networks overlap spatially, with no evidence of divergence of sensory and association networks.

Functional Connectivity Between Mouse Primary Sensory Cortices and Hippocampus Reveals Hippocampal Spatially Localized Sensory Mapping

Although the hippocampus has been the center of anatomical and functional investigations in rodents, a precise functional mapping of different cortical areas in the hippocampus has not been possible heretofore due to the limited ability to image it using optical methods. The modality-specific topography we observed in the parahippocampal region motivated us to leverage fcMRI sensitivity to polysynaptic connectivity to examine whether topographic organization of sensory cortices exists in the hippocampus.

We projected the statistical maps generated by seeds in primary sensory cortices on the flattened surface reconstructions of the hippocampal subfields (Fig. 4) and noted that all 3 primary sensory cortices demonstrated significant correlations. Examining the topography of different modalities, we found that SSp-bfd and VISp are connected preferentially to the dorsal aspect, while AUDp is connected preferentially to the ventral aspect of the hippocampus. To validate that this pattern is consistent across mice, we examined the reproducibility of this topography and found close agreement across animals (Supplementary Fig. 6).

To better characterize topographic organization, we divided each hippocampal subfield into 5 longitudinal segments (based on the 25 original segments, excluding the first dorsal and last

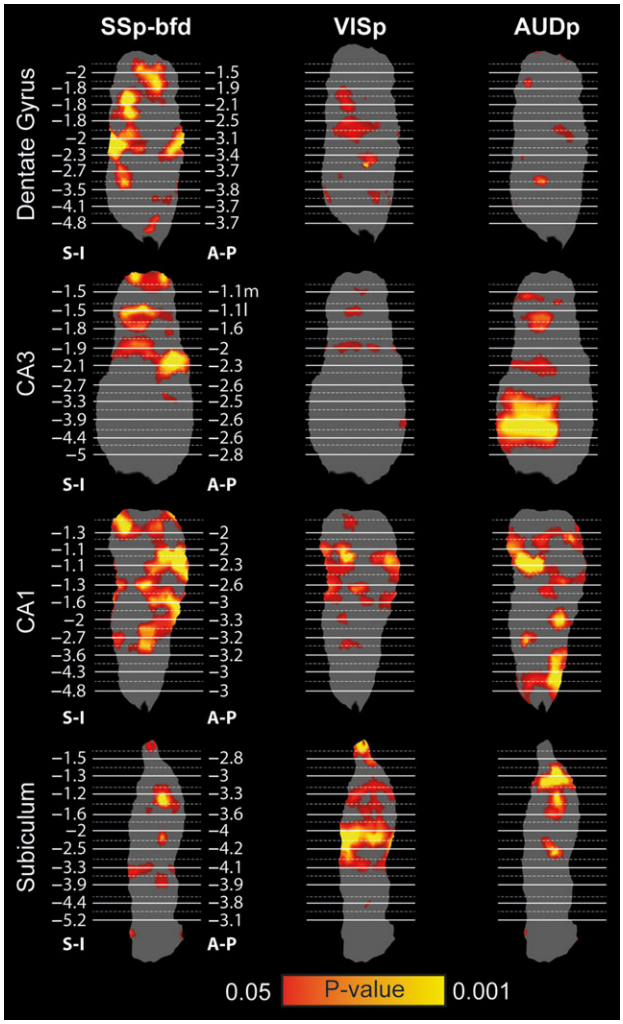

Figure 4. Spatial specificity of sensory cortices mapping on the hippocampus. Statistical maps of barrel-related primary somatosensory (SSp-bfd, left), primary visual (VISp, center), and primary auditory (AUDp, right) cortices mounted on surface reconstructions of the right dentate gyrus, CA3, CA1 and subiculum reveal distinct topography ($P < 0.05$, corrected for multiple comparisons using family-wise error rate correction for the hippocampal memory system).

4 ventral segments due to poor SNR), and calculated the average correlation values of each segment for each seed and subfield (Fig. 5A). The results showed that the peak correlations of different sensory modalities are biased to different longitudinal segments in the dentate gyrus, CA3 and CA1, as SSp-bfd and VISp are more connected to the dorsal-intermediate aspect, while AUDp is more connected to the ventral aspect. To confirm this observation, these results were submitted to repeated measures ANOVA conducted for each subfield, with Longitudinal Sections correlation as repeated measures and Seed Region and Subfield as within animal factors. The results revealed significant interactions between Seed Region and Longitudinal Section ($F_{(8,88)} = 3.14$, $P = 0.004$, $\varepsilon_{H\text{-}F} = 1$), Subfield and Longitudinal Section ($F_{(12,132)} = 2.32$, $P = 0.043$, $\varepsilon_{H\text{-}F} = 0.497$), Seed Region and Subfield ($F_{(6,66)} = 3.63$, $P = 0.019$, $\varepsilon_{H\text{-}F} = 0.553$), and most importantly 3-way interaction between Seed Region, Subfield and Longitudinal Section ($F_{(12,264)} = 6.35$, $P < 0.001$, $\varepsilon_{H\text{-}F} = 1$). These results indicate preferential connectivity of different sensory cortices to different segments along the longitudinal axis of the mouse hippocampus. To break down this 3-way interaction, we conducted follow-up analyses, corrected for multiple comparisons using false-discovery rate (Benjamini and Hochberg 1995) and examined interactions between different pairs of seeds along the longitudinal axis in each subfield separately (Fig. 5B, full statistics are described in Supplementary Table 5). Comparing SSp-bfd and AUDp, the results show interactions between Seed Region and Longitudinal Section across all subfields, especially in the CA fields. In addition, the CA fields also demonstrated interactions between VISp and AUDp connectivity and Longitudinal Section. Finally, no differences in connectivity along the longitudinal axis were found for SSp-bfd and VISp. Together, these results imply that sensory information is only partly integrated in the parahippocampal region and that the relative contribution of different sensory modalities differs along the longitudinal axis. In addition, these findings are in close agreement with previous studies that reported impairments in contextual and auditory fear conditioning following lesions to the dorsal and ventral hippocampus, respectively (Maren and Holt 2004; Yoon and Otto 2007).

Comparative Analysis of Cortico-Hippocampal Connectivity in Mice and Humans

To formally compare cortico-hippocampal connectivity across species, we placed seeds throughout mouse and human cortices. In the mouse, we examined sensory and association cortical seeds (Fig. 6A), plotted the parahippocampal coverage (PRC and POR) versus the hippocampal coverage (Fig. 6B), and found significant correlation ($r_{(14)} = 0.53$, $P = 0.033$), in agreement with the strong anatomical connections between these structures in rodents (Furtak et al. 2007; Kerr et al. 2007). Comparing between different cortical systems, we discovered preferential representation of sensory relative to association cortices in both the parahippocampal region (Mann–Whitney U-test: $U = 5.5$, $P = 0.006$) and hippocampus ($U = 9$, $P = 0.017$).

Given the cortico-hippocampal connectivity in the mouse brain, we sought to compare mouse to human connectivity directly. We divided the seeds into 3 categories (Fig. 6C)—sensory, default/memory, and attention/control—and replicated the hippocampal-parahippocampal coverage analysis (Fig. 6D). We observed that similar to the mouse analysis, cortical functional connectivity to the human parahippocampal region and hippocampus are highly correlated ($r_{(104)} = 0.87$; $P < 0.001$). However, distinct from the mouse, a large fraction of cortical seeds did not exhibit significant correlation to the parahippocampal region (46.22%) nor to the hippocampus (40.56%). Examining the distribution of hippocampal and parahippocampal functional connectivity in each category (Fig. 6E), we found preferential connectivity of default association areas over sensory (Mann–Whitney U-test: parahipocampal region: $U = 412$, $P = 0.011$; hippocampus: $U = 272$, $P < 0.001$) and attention/control association (parahipocampal region: $U = 239.5$, $P < 0.001$; hippocampus: $U = 119$, $P < 0.001$) cortices. In addition, we discovered that sensory functional connectivity to the human hippocampus and parahippocampal regions exists and is significantly higher compared with attention/control association cortices (parahipocampal region: $U = 410$, $P = 0.002$; hippocampus: $U = 398.5$, $P = 0.002$).

Next, we sought to evaluate the hierarchical organization of sensory functional connectivity to the human hippocampus. We used the visual system as a model and plotted the hippocampal and parahippocampal functional connectivity versus the seed location on the anterior–posterior axis ($n = 14$), assuming that more anterior seeds represent higher-order areas in the visual stream. We found significant correlations between

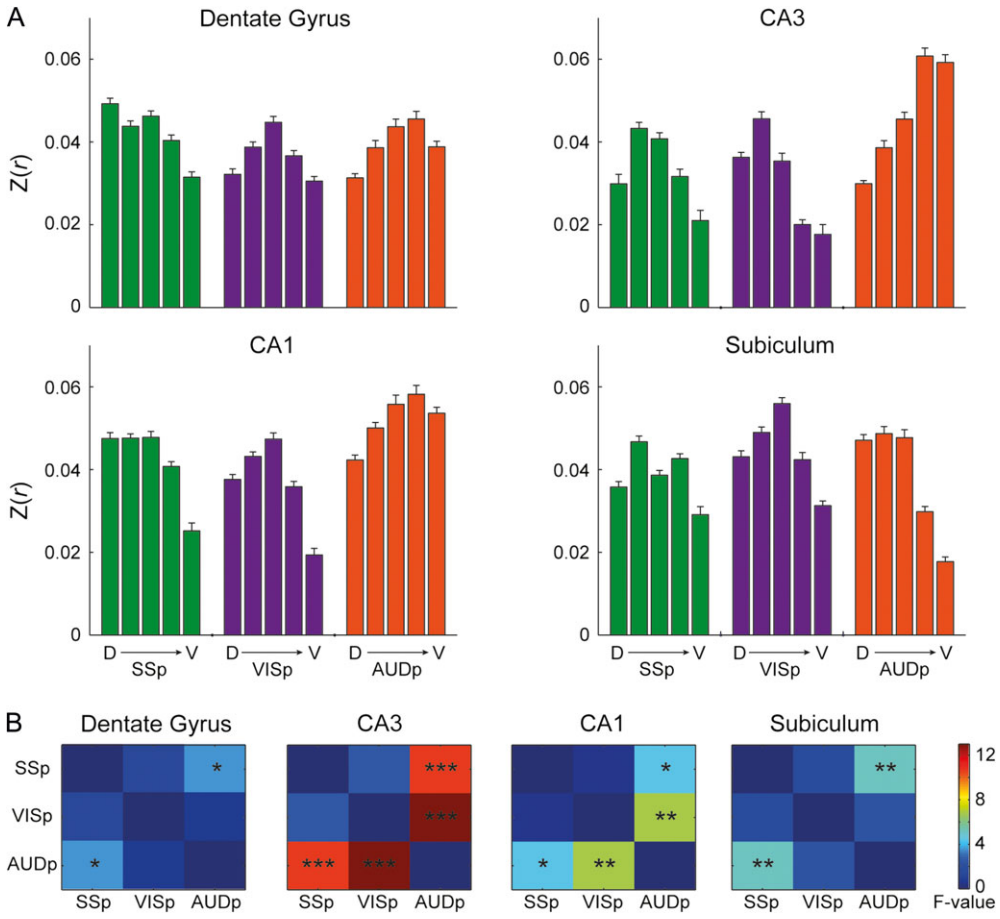

Figure 5. Preferential connectivity of sensory cortices along the hippocampal longitudinal axis. (*A*) Quantification of the correlations of primary sensory cortices to 5 segments along the longitudinal axis of the dentate gyrus, CA3, CA1, and subiculum demonstrates sensory mapping. We excluded the first dorsal-most and 4 ventral-most segments from the original segmentation and averaged the correlations in groups of 4 segments to create a total of 5 segments. Error bars indicate standard error of the mean. (*B*) Quantification of the interaction between pairs of seed regions and longitudinal axis along the hippocampal circuit. *$P < 0.05$, **$P < 0.01$, ***$P < 0.001$, corrected for multiple comparisons using the false-discovery rate method.

parahippocampal ($r_{(12)} = 0.65$, $P = 0.012$) and hippocampal ($r_{(12)} = 0.84$, $P < 0.001$) representations and location along the anterior–posterior axis (Fig. 6*F*). The minimal functional connectivity of posterior visual areas suggests that early visual cortices are connected only weakly to the human hippocampus, as opposed to our findings in mice.

To validate that cross-species differences do not stem from the whole-brain regression used only in humans, we replicated the human analysis without whole-brain regression (Supplementary Fig. 7) and found that it eliminates the difference between default and sensory functional connectivities in the parahippocampal region, but the differential connectivity in the hippocampus is independent of this procedure. A possible explanation for the discrepancy in the parahippocampal region is the strong representation of the whole-brain signal in sensory cortices, specifically the visual cortex (Fox et al. 2009). Moreover, a previous study demonstrated strong correlations between default and visual areas without regression of the whole-brain signal (Murphy et al. 2009), indicating that whole-brain regression enhances specificity in human fcMRI data, as opposed to our observation in mice.

Finally, since human cortical parcellation is not consensual, we replicated this analysis based on an alternative functional clustering (Yeo et al. 2011) and found that the results are also consistent with this clustering approach (Supplementary Fig. 8). Collectively, our findings reveal a dramatic difference between mice and humans since the mouse hippocampus demonstrates preferential functional connectivity to sensory cortices, while the human hippocampus demonstrates bias towards default association cortices, suggesting that rerouting of sensory information through association cortices occurred in humans.

Fractionation of Sensory and Association Networks in the Human Parahippocampal Region

Since we found a transition from sensory to association cortico-hippocampal connectivity and since cortical expansion affected mainly association cortices (Wise 2008; Cooke et al. 2013), we sought to test whether association networks emerged between sensory networks and the hippocampus. Therefore, we examined whether sensory and association networks diverge within the human parahippocampal region compared with the spatial convergence we found in mice.

In a previous fcMRI study (Kahn et al. 2008), spatially localized functional organization of the default and anterior temporal association networks in the human parahippocampal region was shown since inferior parietal and inferior temporal seeds demonstrated differential connectivity to caudal/

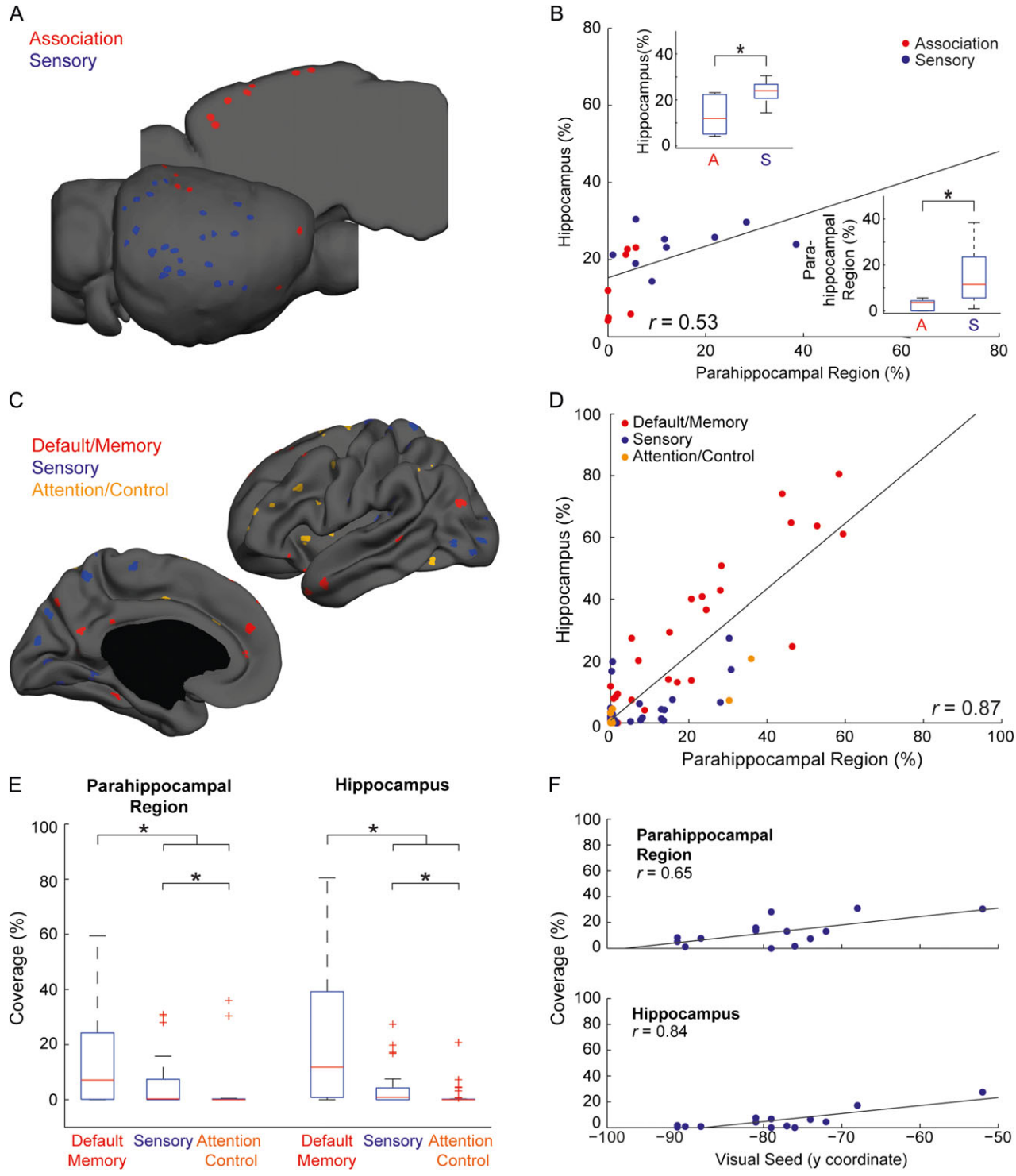

Figure 6. Comparative functional connectivity of the hippocampal memory system. (*A*) Seed locations in mouse cortex. (*B*) Quantification of the hippocampal versus parahippocampal functional connectivity to different regions in the mouse cortex reveals significant correlation and weaker functional connectivity of association cortices. The distributions of coverage for each category are shown in boxplots and demonstrate stronger representation of sensory compared to association cortices in the mouse parahippocampal region and hippocampus ($P < 0.05$). (*C*) Seed locations in the human cortex. (*D*) Quantification of hippocampal versus parahippocampal functional connectivity to different regions in the human cortex reveals corresponding correlations in these 2 structures. (*E*) Boxplots of hippocampal and parahippocampal representations of different cortical systems in humans reveal stronger representation of default/memory over sensory and attention/control cortices, as well as preferential connectivity of sensory over attention/control areas. Significant differences ($P < 0.05$) are marked with asterisks. (*F*) Quantification of hippocampal and parahippocampal functional connectivity versus seed location within the visual system reveals strong correlations that indicate hierarchical organization.

intermediate PHC and rostral PHC/PRC, respectively. However, since the whole-brain analysis was based on specific seeds, it might have represented a conservative estimate of sensory connectivity, explaining its lack thereof. More recently, Baldassano et al. (2013) examined the connectivity of visual and default association areas within the PHC during object-in-scene and scene-category tasks, demonstrating a transition of functional connectivity between caudal and rostral PHC. Motivated by the coverage analysis, we sought to examine the spatial organization of sensory and association cortical networks in the human parahippocampal region using intrinsic functional connectivity data to compare the results directly to mice.

Examination of representative human fcMRI maps of a visual seed in area V2 (Fig. 7A; seed #167) and an association seed in the posterior cingulate cortex (PCC; Fig. 7B; seed #88) shows differential connectivity within the PHC since V2 is connected to its caudal aspect, while PCC is connected to its intermediate and rostral aspects. To confirm this result, we placed 3 seeds along the longitudinal axis of the parahippocampal cortex (Fig. 7C; Supplementary Table 6), calculated the average correlation of each seed to V2 and PCC seeds, and submitted the results to a repeated-measures ANOVA, with Seed Region as a within animal factor and correlation values of the 3 Longitudinal Sections as repeated measures. This analysis revealed a significant interaction between Seed Region and Longitudinal Sections ($F_{(2,\ 86)} = 43.53$, $P < 0.001$, $\varepsilon_{H\text{-}F} = 0.848$). Post-hoc paired t-tests revealed significantly higher correlation of V2 (0.17 ± 0.18, mean $\pm$ SD) over PCC (0.07 ± 0.15) in the caudal seed (paired t-test: $t_{(43)} = 2.52$, $P = 0.015$) compared with significantly higher correlation of PCC (0.18 ± 0.13) over V2 (0.017 ± 0.12) in the rostral seed ($t_{(43)} = 6.22$, $P < 0.001$), indicating differential connectivity. To generalize this conclusion from a specific pair of seeds to the network level, we calculated the fraction of statistically significant vertices for 10 sensory and default seeds with the higher hippocampal coverage, and found that the result is consistent within each group of seeds (Fig. 7D). In addition, conducting the reciprocal analysis, we examined the whole-brain connectivity of the caudal and rostral seeds, and found a transition from the visual to the default network (Fig. 7E), confirming spatial divergence of sensory and association networks in the human parahippocampal region.

Anatomical studies in nonhuman primates divide the parahippocampal cortex into 3 distinct subregions (TFO, TF and TH) with differential anatomical connectivity (Suzuki and Amaral 2003; Suzuki 2009; Kravitz et al. 2011). While caudal TEO receives dense projections from visual areas V4 and TE, rostral TF and TH receive only mild visual projections. In contrast, parietal, temporal and frontal association areas project to all subregions. Our results show that fcMRI captures these anatomical patterns, demonstrating differential connectivity of visual and default association networks along the rostro-caudal axis and indicating fractionation of sensory and association networks in the human parahippocampal region, as opposed to our observations in mice.

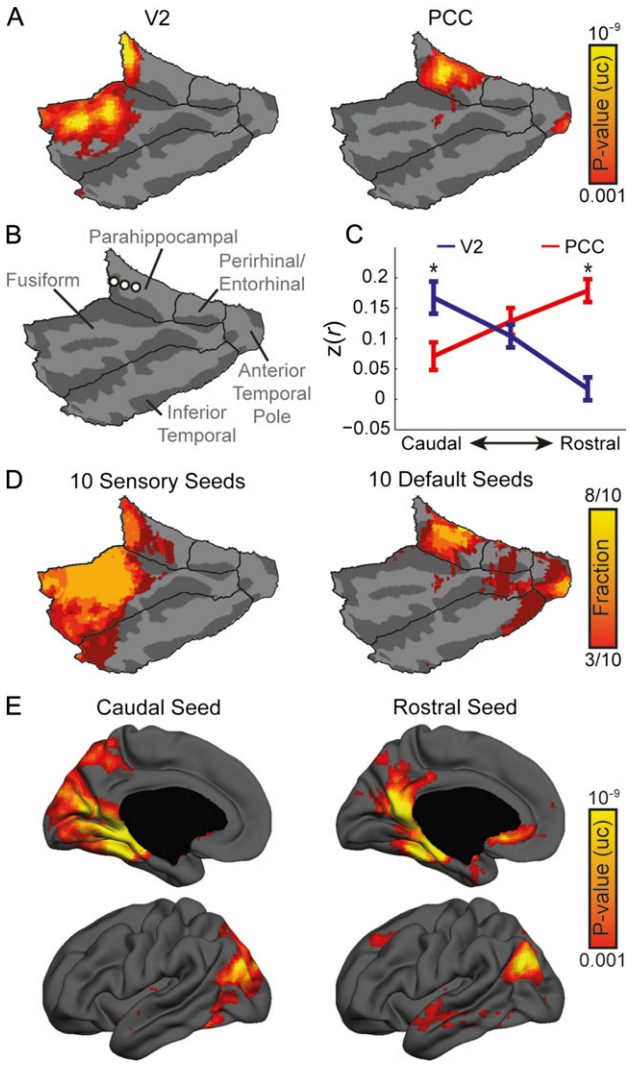

Figure 7. Divergence of sensory and association networks in the human parahippocampal region. (*A*) Cortico-parahippocampal analysis comparing human visual cortex (area V2) to PCC reveals divergence of sensory and association cortices in the human medial temporal lobe, specifically in PHC ($P < 0.001$, uncorrected). (*B*) Location of seeds along the rostro-caudal axis of the left PHC. See Supplementary Table 6 for coordinates in MNI space. (*C*) Correlation values of V2 and PCC to seeds along the rostro-caudal axis of PHC reveal differential connectivity. Asterisks represent significant differences between V2 and PCC correlations ($P < 0.05$). Error bars indicate standard error of the mean. (*D*) Statistically significant fractions of 10 sensory and default association seeds demonstrate consistent divergence within the parahippocampal region. (*E*) Whole-brain connectivity of seeds along the rostro-caudal axis of the parahippocampal region demonstrates transition of connectivity from visual to association networks ($P < 0.001$, uncorrected).

Discussion

We used the slow coherent fluctuations in the BOLD fMRI signal to investigate how expansion and elaboration of the human relative to the mouse cortex impacted cortico-hippocampal connectivity. We observed differential connectivity of sensory and association cortices in the mouse and human hippocampi with a divergence of sensory and association networks in the human but not the mouse parahippocampal region. In contrast, in mice we found sensory mapping in the parahippocampal region that extends to the hippocampus. Collectively, these results show coupling between cortical sensory networks and the hippocampus in the mouse in contrast to dissociation of these networks in the human, indicating rerouting of cortical sensory inputs via association cortices in humans.

Intrinsic Functional Connectivity in the Awake Mouse Brain

We used fcMRI to estimate functional connectivity in the mouse brain and directly compare the results to humans.

While intrinsic functional connectivity is widely used in human neuroimaging studies, it has been limited in use in rodents due to the difficulty to image awake animals and limited spatial resolution afforded by the small rodent brain. Administration of anesthetic agents results in an attenuated fMRI signal, particularly at high resolution (Peltier et al. 2005; Desai et al. 2011). Using a custom-made cradle, we were able to record spontaneous BOLD fMRI fluctuations over multiple sessions and create an extensive dataset for fcMRI investigation. Furthermore, we used SE-EPI rather than the more commonly used gradient-echo EPI (GE-EPI) applied in previous rodent fcMRI studies (Liang et al. 2012; Lu et al. 2012; Grandjean et al. 2014; Mechling et al. 2014; Nasrallah et al. 2014; Sforazzini et al. 2014; Stafford et al. 2014; Shah et al. 2015). While SE-EPI has lower SNR relative to GE-EPI, it is less sensitive to inhomogeneities of the magnetic field, producing less distorted images and enabling better coregistration to a common atlas. In addition, at high magnetic fields, SE-EPI is more sensitive to microvasculature relative to GE-EPI (Uludağ et al. 2009; Budde et al. 2014; Ugurbil 2014), enabling a high contrast-to-noise ratio for functional mapping at high resolutions (Yacoub et al. 2008). Moreover, in the context of fcMRI, SE-EPI was shown to be as sensitive and specific as GE-EPI and provided superior results in high-susceptibility regions (Koopmans et al. 2012; Khatamian et al. 2016). Finally, in mice, we and others (Zerbi et al. 2014) demonstrated that SE-EPI recapitulates homotopicity, which is the hallmark of fcMRI in rodents. Collectively, these advantages allowed investigation of high-resolution whole-brain functional connectivity, including the parahippocampal region, which is highly sensitive to susceptibility artifacts, as well as a comparison to the AMBC Atlas. This comparison allowed us to estimate structure–function relations virtually at a single voxel resolution, enabling multimodal characterization of mesocopic organization of the mouse brain.

In addition to structure–function analysis in the mouse brain, mouse fcMRI is a powerful method for translational and comparative studies. While the biological origin of intrinsic functional connectivity is yet to be discovered, previous studies reported that this approach is in close agreement to anatomical connectivity (Mohajerani et al. 2013; Stafford et al. 2014) and has an electrophysiological substrate (Wang et al. 2013). Moreover, the fact that intrinsic connectivity does not require any active participation eliminates many confounds related to behavioral comparisons. In this study, we tried to conduct the identical preprocessing procedure in both datasets, avoiding the addition of any methodological confounds. However, we found that global signal regression eliminates correlations in the mouse brain, while in humans this step enhances specificity (Fox et al. 2009; Murphy et al. 2009). We hypothesized that this effect is a result of the less segregated mouse brain as virtually all structures are connected within 2–3 synapses. Nevertheless, we confirmed that the cross-species differences we found are independent of this preprocessing step, suggesting that while fcMRI is an imperfect method, it still provides a useful tool for cross-species comparisons, and is specifically useful for comparing cortico-hippocampal connectivity as it bridges between anatomical studies in rodents to functional studies in humans.

Functional Coupling Between Sensory Networks and the Hippocampal Memory System in the Mouse Brain

The central finding of this study is the putative functional coupling between primary sensory cortices and the hippocampal memory system in the mouse. Previous anatomical tracing studies showed that primary and secondary sensory cortices map to distinct subregions within the mouse parahippocampal region (Burwell and Amaral 1998b; Furtak et al. 2007; Agster and Burwell 2013), and characterized the anatomical projections from the parahippocampal region and the hippocampus (Furtak et al. 2007; Kerr et al. 2007; Agster and Burwell 2013). However, since the connections between primary sensory cortices and the hippocampus are polysynaptic, they were not examined using traditional tracing methods. Here, we utilized the sensitivity of fcMRI to polysynaptic connections to characterize cortico-hippocampal functional connectivity.

The fcMRI data capture the sensory mapping in the mouse parahippocampal region and show that the topographic organization extends to the hippocampus, demonstrating segregation of somatosensory/visual and auditory inputs along the longitudinal axis. While previous studies showed that the rodent hippocampus responds to pure sensory stimuli (Pereira et al. 2007; Vinnik et al. 2012) and found some evidence of preferential responses in distinct subregions within CA1 (Bellistri et al. 2013), sensory processing in the mouse hippocampus is still poorly understood. Nevertheless, a recent study (Haggerty and Ji 2015) described correlated activity in primary visual cortical neurons and spatially selective CA1 neurons during navigation in rats, suggesting that information processed in visual cortex is the substrate for the visual component of long-term spatial memories. In addition, increased coherent activity in dorsal hippocampus and barrel-related primary somatosensory cortex was shown to facilitate the integration of tactile information into memory during the tactile discrimination task (Grion et al. 2016). Our results correspond to these observations, demonstrating strong functional connectivity between primary sensory cortices and the hippocampus.

Cortical Rerouting Dissociates the Human Hippocampus From Primary Sensory Cortices

Previous cross-species comparisons characterized phylogenetic changes in the hippocampal memory system. These studies found that the hippocampal formation in amphibians is directly connected to the dorsal thalamus (Roth et al. 2003; Laberge and Roth 2007), and that these thalamo-hippocamapal connections weakened in reptiles (Guirado and Dávila 2002) and disappeared in mammals, demonstrating cortical rerouting of sensory input through the cerebral cortex (Striedter 2005). Our results show that the set of brain regions involved in sensory and memory processing is coupled in mice, but as reflected by fcMRI, demonstrates distinctly reduced functional connectivity in humans. This divergence indicates the possibility of another rerouting event occurring in the human cortex relative to rodents in which cortical sensory inputs pass through expanded and new association cortices before arriving at the hippocampus.

Taking into account the differential representation of sensory relative to association networks in mouse and human brains (Krubitzer 2009; Buckner and Krienen 2013), the topographic organization of different sensory modalities within the mouse hippocampal memory system and the divergence of sensory and association networks in the human parahippocampal region, we propose that as opposed to humans, the cortico-hippocampal network in mice represents a single hierarchy. The mouse hippocampus operates on inputs that are closely associated to the physical features of external stimuli, rather than abstract information that emerges after several stages of processing. In contrast, in humans, noncanonical association

network hierarchies emerged between canonical sensory hierarchies and the hippocampal memory system. Namely, cortical expansion and the emergence of new association areas in humans resulted in the fractionation of the primary sensory areas and the hippocampal memory system, as observed with fcMRI. The functional significance of this fractionation requires further investigation, but based on our analyses, we would like to propose that the divergent cortico-hippocampal connectivity might underlie qualitatively different sensory inputs to the mouse and human hippocampi that subserve different hippocampal-dependent memory representations.

Supplementary Material

Supplementary material can be found at: http://www.cercor.oxfordjournals.org/

Funding

The Israel Science Foundation 225/11 (I.K.), the Israel Ministry of Science and Technology 3-10373 (I.K.), the European Research Council PCIG9-GA-2011-294001 (I.K.), the Adelis Foundation, and the Allen and Jewel Prince Center for Neurodegenerative Processes of the Brain.

Notes

We thank Daphna Shohamy and Mark Andermann for their helpful comments on the manuscript, Guennady Yudkovsky for his fine machining and rapid prototyping assistance, Technion's Biological Core Facilities and Edith Suss-Toby for her assistance with the MRI, and the Technion Preclinical Research Authority and Nadav Cohen for assistance with animal care. *Conflict of Interest*: None declared.

References

Agster KL, Burwell RD. 2013. Hippocampal and subicular efferents and afferents of the perirhinal, postrhinal, and entorhinal cortices of the rat. Behav Brain Res. 254:50–64.

Allen TA, Fortin NJ. 2013. The evolution of episodic memory. Proc Natl Acad Sci USA. 110(Suppl):10379–10386.

Aronoff R, Matyas F, Mateo C, Ciron C, Schneider B, Petersen CCH. 2010. Long-range connectivity of mouse primary somatosensory barrel cortex. Eur J Neurosci. 31:2221–2233.

Baldassano C, Beck DM, Fei-Fei L. 2013. Differential connectivity within the parahippocampal place area. Neuroimage. 75: 228–237.

Beaudin SA, Singh T, Agster KL, Burwell RD. 2013. Borders and comparative cytoarchitecture of the perirhinal and postrhinal cortices in an F1 hybrid mouse. Cereb Cortex. 23: 460–476.

Bellistri E, Aguilar J, Brotons-Mas JR, Foffani G, de la Prida LM. 2013. Basic properties of somatosensory-evoked responses in the dorsal hippocampus of the rat. J Physiol. 591: 2667–2686.

Benjamini Y, Hochberg Y. 1995. Controlling the false discovery rate: a practical and powerful approach to multiple testing. J R Stat Soc Ser B. 57:289–300.

Buckner RL, Krienen FM. 2013. The evolution of distributed association networks in the human brain. Trends Cogn Sci. 17:648–665.

Buckner RL, Krienen FM, Yeo BTT. 2013. Opportunities and limitations of intrinsic functional connectivity MRI. Nat Neurosci. 16:832–837.

Budde J, Shajan G, Zaitsev M, Scheffler K, Pohmann R. 2014. Functional MRI in human subjects with gradient-echo and spin-echo EPI at 9.4 T. Magn Reson Med. 71:209–218.

Burwell RD. 2000. The parahippocampal region: corticocortical connectivity. Ann NY Acad Sci. 911:25–42.

Burwell RD, Agster KL. 2008.Anatomy of the hippocampus and the declarative memory system. In: Eichenbaum HE, editor. Memory systems. Oxford: Elsevier. p. 47–66.

Burwell RD, Amaral DG. 1998a. Perirhinal and postrhinal cortices of the rat: interconnectivity and connections with the entorhinal cortex. J Comp Neurol. 391:293–321.

Burwell RD, Amaral DG. 1998b. Cortical afferents of the perirhinal, postrhinal, and entorhinal cortices of the rat. J Comp Neurol. 398:179–205.

Cooke DF, Goldring A, Recanzone GH, Krubitzer L. 2013. The evolution of parietal areas associated with visuomanual behavior: from grasping to tool use. In: Werner JS, Chalupa LM, editors. The visual neurosciences. Cambridge (MA): MIT Press. p. 1049–1063.

Dale AM, Fischl B, Sereno MI. 1999. Cortical surface-based analysis. I. Segmentation and surface reconstruction. Neuroimage. 9:179–194.

Desai M, Kahn I, Knoblich U, Bernstein J, Atallah H, Yang A, Kopell N, Buckner RL, Graybiel AM, Moore CI, et al. 2011. Mapping brain networks in awake mice using combined optical neural control and fMRI. J Neurophysiol. 105:1393–1405.

Eichenbaum H. 2000. A cortical-hippocampal system for declarative memory. Nat Rev Neurosci. 1:41–50.

Fischl B, Sereno MI, Dale AM. 1999. Cortical surface-based analysis. II: Inflation, flattening, and a surface-based coordinate system. Neuroimage. 9:195–207.

Fox MD, Zhang D, Snyder AZ, Raichle ME. 2009. The global signal and observed anticorrelated resting state brain networks. J Neurophysiol. 101:3270–3283.

Furtak SC, Wei S-M, Agster KL, Burwell RD. 2007. Functional neuroanatomy of the parahippocampal region in the rat: the perirhinal and postrhinal cortices. Hippocampus. 17:709–722.

Gass N, Schwarz AJ, Sartorius A, Schenker E, Risterucci C, Spedding M, Zheng L, Meyer-Lindenberg A, Weber-Fahr W. 2014. Sub-anesthetic ketamine modulates intrinsic BOLD connectivity within the hippocampal-prefrontal circuit in the rat. Neuropsychopharmacology. 39:895–906.

Geschwind DH, Rakic P. 2013. Cortical evolution: judge the brain by its cover. Neuron. 80:633–647.

Gozzi A, Schwarz AJ. 2016. Large-scale functional connectivity networks in the rodent brain. Neuroimage. 127:496–509.

Grandjean J, Schroeter A, Batata I, Rudin M. 2014. Optimization of anesthesia protocol for resting-state fMRI in mice based on differential effects of anesthetics on functional connectivity patterns. Neuroimage. 102P2:838–847.

Grion N, Akrami A, Zuo Y, Stella F, Diamond ME. 2016. Coherence between rat sensorimotor system and hippocampus is enhanced during tactile discrimination. PLoS Biol. 14: e1002384.

Guirado S, Dávila JC. 2002. Thalamo-telencephalic connections: new insights on the cortical organization in reptiles. Brain Res Bull. 57:451–454.

Guo ZV, Hires SA, Li N, O'Connor DH, Komiyama T, Ophir E, Huber D, Bonardi C, Morandell K, Gutnisky D, et al. 2014. Procedures for behavioral experiments in head-fixed mice. PLoS One. 9:e88678.

Haggerty DC, Ji D. 2015. Activities of visual cortical and hippocampal neurons co-fluctuate in freely moving rats during spatial navigation. Elife. 4:e08902.

Ho JW, Burwell RD. 2014. Perirhinal and postrhinal functional inputs to the hippocampus. In: Space, time and memory in the hippocampal formation. Vienna: Springer. p. 55–81.

Kahn I, Andrews-Hanna JR, Vincent JL, Snyder AZ, Buckner RL. 2008. Distinct cortical anatomy linked to subregions of the medial temporal lobe revealed by intrinsic functional connectivity. J Neurophysiol. 100:129–139.

Kahn I, Desai M, Knoblich U, Bernstein J, Henninger M, Graybiel AM, Boyden ES, Buckner RL, Moore CI. 2011. Characterization of the functional MRI response temporal linearity via optical control of neocortical pyramidal neurons. J Neurosci. 31:15086–15091.

Kerr KM, Agster KL, Furtak SC, Burwell RD. 2007. Functional neuroanatomy of the parahippocampal region: the lateral and medial entorhinal areas. Hippocampus. 17:697–708.

Khatamian YB, Golestani AM, Ragot DM, Chen JJ. 2016. Spin-echo resting-state functional connectivity in high-susceptibility regions: accuracy, reliability, and the impact of physiological noise. Brain Connect. 6:283–297.

Koopmans PJ, Boyacioğlu R, Barth M, Norris DG. 2012. Whole brain, high resolution spin-echo resting state fMRI using PINS multiplexing at 7 T. Neuroimage. 62:1939–1946.

Kravitz DJ, Saleem KS, Baker CI, Mishkin M. 2011. A new neural framework for visuospatial processing. Nat Rev Neurosci. 12:217–230.

Krubitzer L. 2009. In search of a unifying theory of complex brain evolution. Ann NY Acad Sci. 1156:44–67.

Laberge F, Roth G. 2007. Organization of the sensory input to the telencephalon in the fire-bellied toad, Bombina orientalis. J Comp Neurol. 502:55–74.

Lein ES, Hawrylycz MJ, Ao N, Ayres M, Bensinger A, Bernard A, Boe AF, Boguski MS, Brockway KS, Byrnes EJ, et al. 2007. Genome-wide atlas of gene expression in the adult mouse brain. Nature. 445:168–176.

Liang Z, King J, Zhang N. 2012. Anticorrelated resting-state functional connectivity in awake rat brain. Neuroimage. 59: 1190–1199.

Libby LA, Ekstrom AD, Ragland JD, Ranganath C. 2012. Differential connectivity of perirhinal and parahippocampal cortices within human hippocampal subregions revealed by high-resolution functional imaging. J Neurosci. 32: 6550–6560.

Liska A, Galbusera A, Schwarz AJ, Gozzi A. 2015. Functional connectivity hubs of the mouse brain. Neuroimage. 115: 281–291.

Lu H, Zou Q, Gu H, Raichle ME, Stein EA, Yang Y. 2012. Rat brains also have a default mode network. Proc Natl Acad Sci USA. 109:3979–3984.

Manns JR, Eichenbaum H. 2006. Evolution of declarative memory. Hippocampus. 16:795–808.

Maren S, Holt WG. 2004. Hippocampus and Pavlovian fear conditioning in rats: muscimol infusions into the ventral, but not dorsal, hippocampus impair the acquisition of conditional freezing to an auditory conditional stimulus. Behav Neurosci. 118:97–110.

Mechling AE, Hübner NS, Lee H-L, Hennig J, von Elverfeldt D, Harsan L-A. 2014. Fine-grained mapping of mouse brain functional connectivity with resting-state fMRI. Neuroimage. 96:203–215.

Mohajerani MH, Chan AW, Mohsenvand M, LeDue J, Liu R, McVea DA, Boyd JD, Wang YT, Reimers M, Murphy TH. 2013. Spontaneous cortical activity alternates between motifs defined by regional axonal projections. Nat Neurosci. 16:1426–1435.

Murphy K, Birn RM, Handwerker DA, Jones TB, Bandettini PA. 2009. The impact of global signal regression on resting state correlations: are anti-correlated networks introduced? Neuroimage. 44:893–905.

Nasrallah FA, Tay H-C, Chuang K-H. 2014. Detection of functional connectivity in the resting mouse brain. Neuroimage. 86:417–424.

Navarro Schröder T, Haak KV, Zaragoza Jimenez NI, Beckmann CF, Doeller CF. 2015. Functional topography of the human entorhinal cortex. Elife. 4:e06738.

Neunuebel JP, Yoganarasimha D, Rao G, Knierim JJ. 2013. Conflicts between local and global spatial frameworks dissociate neural representations of the lateral and medial entorhinal cortex. J Neurosci. 33:9246–9258.

Norman G, Eacott MJ. 2005. Dissociable effects of lesions to the perirhinal cortex and the postrhinal cortex on memory for context and objects in rats. Behav Neurosci. 119:557–566.

Oh SW, Harris JA, Ng L, Winslow B, Cain N, Mihalas S, Wang Q, Lau C, Kuan L, Henry AM, et al. 2014. A mesoscale connectome of the mouse brain. Nature. 508:207–214.

Paxinos G, Franklin KBJ. 2001. The mouse brain in stereotaxic coordinates. 2nd ed. San Diego: Academic Press.

Peltier SJ, Kerssens C, Hamann SB, Sebel PS, Byas-Smith M, Hu X. 2005. Functional connectivity changes with concentration of sevoflurane anesthesia. Neuroreport. 16:285–288.

Pereira A, Ribeiro S, Wiest M, Moore LC, Pantoja J, Lin S-C, Nicolelis MAL. 2007. Processing of tactile information by the hippocampus. Proc Natl Acad Sci USA. 104:18286–18291.

Power JD, Cohen AL, Nelson SM, Wig GS, Barnes KA, Church JA, Vogel AC, Laumann TO, Miezin FM, Schlaggar BL, et al. 2011. Functional network organization of the human brain. Neuron. 72:665–678.

Power JD, Mitra A, Laumann TO, Snyder AZ, Schlaggar BL, Petersen SE. 2014a. Methods to detect, characterize, and remove motion artifact in resting state fMRI. Neuroimage. 84:320–341.

Power JD, Schlaggar BL, Petersen SE. 2014b. Studying brain organization via spontaneous fMRI signal. Neuron. 84: 681–696.

Rakic P. 2009. Evolution of the neocortex: a perspective from developmental biology. Nat Rev Neurosci. 10: 724–735.

Ranganath C, Ritchey M. 2012. Two cortical systems for memory-guided behaviour. Nat Rev Neurosci. 13:713–726.

Roth G, Grunwald W, Dicke U. 2003. Morphology, axonal projection pattern, and responses to optic nerve stimulation of thalamic neurons in the fire-bellied toad Bombina orientalis. J Comp Neurol. 461:91–110.

Schwarz AJ, Gass N, Sartorius A, Zheng L, Spedding M, Schenker E, Risterucci C, Meyer-Lindenberg A, Weber-Fahr W. 2013. The low-frequency blood oxygenation level-dependent functional connectivity signature of the hippocampal–prefrontal network in the rat brain. Neuroscience. 228:243–258.

Sforazzini F, Schwarz AJ, Galbusera A, Bifone A, Gozzi A. 2014. Distributed BOLD and CBV-weighted resting-state networks in the mouse brain. Neuroimage. 87:403–415.

Shah D, Blockx I, Guns P-J, De Deyn PP, Van Dam D, Jonckers E, Delgado Y, Palacios R, Verhoye M, Van der Linden A. 2015. Acute modulation of the cholinergic system in the mouse brain detected by pharmacological resting-state functional MRI. Neuroimage. 109:151–159.

Stafford JM, Jarrett BR, Miranda-Dominguez O, Mills BD, Cain N, Mihalas S, Lahvis GP, Lattal KM, Mitchell SH, David SV, et al. 2014. Large-scale topology and the default mode network in the mouse connectome. Proc Natl Acad Sci USA. 111:201404346.

Striedter GF. 2005. Principles of brain evolution. Sunderland: Sinauer.

Suzuki WA. 2009.Comparative analysis of the cortical afferents, intrinsic projections and interconnections of the parahippocampal region in monkeys and rats. In: Gazzaniga MS, editor. The cognitive neurosciences. 4th ed. Cambridge (MA): MIT Press. p. 659–674.

Suzuki WA, Amaral DG. 2003. Perirhinal and parahippocampal cortices of the Macaque monkey: cytoarchitectonic and chemoarchitectonic organization. J Comp Neurol. 463:67–91.

Ugurbil K. 2014. Magnetic resonance imaging at ultrahigh fields. IEEE Trans Biomed Eng. 61:1364–1379.

Uludağ K, Müller-Bierl B, Uğurbil K. 2009. An integrative model for neuronal activity-induced signal changes for gradient and spin echo functional imaging. Neuroimage. 48:150–165.

van Strien NM, Cappaert NLM, Witter MP. 2009. The anatomy of memory: an interactive overview of the parahippocampal-hippocampal network. Nat Rev Neurosci. 10:272–282.

Vinnik E, Antopolskiy S, Itskov PM, Diamond ME. 2012. Auditory stimuli elicit hippocampal neuronal responses during sleep. Front Syst Neurosci. 6:49.

Wang Q, Sporns O, Burkhalter A. 2012. Network analysis of corticocortical connections reveals ventral and dorsal processing streams in mouse visual cortex. J Neurosci. 32:4386–4399.

Wang Z, Chen LM, Négyessy L, Friedman RM, Mishra A, Gore JC, Roe AW. 2013. The relationship of anatomical and functional connectivity to resting-state connectivity in primate somatosensory cortex. Neuron. 78:1116–1126.

Wise SP. 2008. Forward frontal fields: phylogeny and fundamental function. Trends Neurosci. 31:599–608.

Yacoub E, Harel N, Ugurbil K. 2008. High-field fMRI unveils orientation columns in humans. Proc Natl Acad Sci USA. 105:10607–10612.

Yeo BTT, Krienen FM, Sepulcre J, Sabuncu MR, Lashkari D, Hollinshead M, Roffman JL, Smoller JW, Zöllei L, Polimeni JR, et al. 2011. The organization of the human cerebral cortex estimated by intrinsic functional connectivity. J Neurophysiol. 106:1125–1165.

Yoon T, Otto T. 2007. Differential contributions of dorsal vs. ventral hippocampus to auditory trace fear conditioning. Neurobiol Learn Mem. 87:464–475.

Zar JH. 1996. Biostatistical analysis. Upper Saddle River: Prentice Hall.

Zerbi V, Wiesmann M, Emmerzaal TL, Jansen D, Van Beek M, Mutsaers MPC, Beckmann CF, Heerschap A, Kiliaan AJ. 2014. Resting-state functional connectivity changes in aging apoE4 and apoE-KO mice. J Neurosci. 34: 13963–13975.